

One-dimensional spin liquid, collinear, and spiral phases from uncoupled chains to the triangular lattice

Luca F. Tocchio,^{1,2} Claudius Gros,¹ Roser Valentí,¹ and Federico Becca²

¹*Institute for Theoretical Physics, University of Frankfurt,
Max-von-Laue-Straße 1, D-60438 Frankfurt a.M., Germany*

²*CNR-IOM-Democritos National Simulation Centre and International School
for Advanced Studies (SISSA), Via Bonomea 265, I-34136, Trieste, Italy*

(Dated: June 18, 2021)

We investigate the Hubbard model on the anisotropic triangular lattice with two hopping parameters t and t' in different spatial directions, interpolating between decoupled chains ($t = 0$) and the isotropic triangular lattice ($t = t'$). Variational wave functions that include both Jastrow and backflow terms are used to compare spin-liquid and magnetic phases with different pitch vectors describing both collinear and coplanar (spiral) order. For relatively large values of the on-site interaction $U/t' \gtrsim 10$ and substantial frustration, i.e., $0.3 \lesssim t/t' \lesssim 0.8$, the spin-liquid state is clearly favored over magnetic states. Spiral magnetic order is only stable in the vicinity of the isotropic point, while collinear order is obtained in a wide range of inter-chain hoppings from small to intermediate frustration.

PACS numbers: 71.10.Fd, 71.27.+a, 75.10.-b

I. INTRODUCTION

Since the pioneering work by Fazekas and Anderson 40 years ago,¹ where magnetically disordered states (the so-called spin liquids) have been proposed as alternative ground states to standard ordered phases in magnetic systems, the field of frustrated magnetism has evolved as an important branch in condensed matter physics. The main motivation is that several unconventional features may arise when magnetism is suppressed at very low temperatures, like fractionalization of quantum numbers or topological degeneracy, to mention a few.

After four decades, our understanding on the subject is still rather incomplete: on the theoretical side, more effort is needed to clarify which are the microscopic models that may sustain spin-liquid ground states and which are suitable diagnostics to detect the presence of exotic properties; on the experimental side, it is important to synthesize and characterize new materials that may present both strong electronic interactions and suitable magnetic frustration.

Organic charge-transfer salts, based on molecules like (BEDT-TTF)₂ or Pd(dmit)₂, represent important examples where the interplay between electronic itineracy, strong correlation, and geometrical frustration lead to various interesting phenomena.² In these systems, the building blocks are given by extended molecular orbitals of dimerized molecules that are arranged in stacked triangular lattices. By varying the applied pressure and temperature, as well as the nature of the cation associated to these materials, they may show metallic, superconducting, or insulating properties.^{3,4} Whenever a single orbital for each dimer is considered, the low-temperature behavior of these materials may be captured by a single-band Hubbard model on the anisotropic triangular lattice, with half-filled density, and relatively large on-site Coulomb repulsion.⁴⁻⁶

Besides these organic systems, also Cs₂CuBr₄ and Cs₂CuCl₄ have a crystalline structure in which (magnetic) Copper atoms lie on weakly-coupled triangular lattices. In spite of being isostructural and isoelectronic, these two materials have completely different magnetic behavior. While the Br compound shows spiral magnetic ordering with well-defined magnon excitations,⁷ Cs₂CuCl₄ shows spin-liquid behavior over a broad temperature range with fractional spin excitations as revealed by inelastic neutron scattering experiments.⁸ At very small temperatures, i.e., below $T_N = 0.62K$, the existence of a tiny inter-layer coupling stabilizes a true three-dimensional magnetic order. Also in this case, the low-energy properties of these materials may be captured by considering correlated electrons with highly reduced kinetic energy and strong Coulomb repulsion, possibly including different $3d$ orbitals of the Copper atoms in the Br compound.⁹ Cs₂CuBr₄ and Cs₂CuCl₄ are the end-member compounds of the family Cs₂CuCl_{4-x}Br_x which shows a variety of magnetic properties when x is changed.¹⁰ The distinct low-energy behaviors are generically attributed to the respective different degrees of frustration, which are determined in turn by the respective ratios between the inter-chain and intra-chain couplings in the underlying anisotropic triangular lattice.

Motivated by the rich phenomenology of these materials, we study the single-band Hubbard model on the anisotropic triangular lattice:

$$\mathcal{H} = - \sum_{i,j,\sigma} t_{ij} c_{i,\sigma}^\dagger c_{j,\sigma} + \text{h.c.} + U \sum_i n_{i,\uparrow} n_{i,\downarrow}, \quad (1)$$

where $c_{i,\sigma}^\dagger$ ($c_{i,\sigma}$) creates (destroys) an electron with spin σ on site i and $n_{i,\sigma} = c_{i,\sigma}^\dagger c_{i,\sigma}$ is the electronic density; U is the on-site Coulomb repulsion and t_{ij} is the hopping amplitude, including an intra-chain t' , along $\mathbf{a}_1 = (1, 0)$, and an inter-chain t , along $\mathbf{a}_2 = (1/2, \sqrt{3}/2)$ and $\mathbf{a}_3 = \mathbf{a}_2 - \mathbf{a}_1$, see Fig. 1(a).

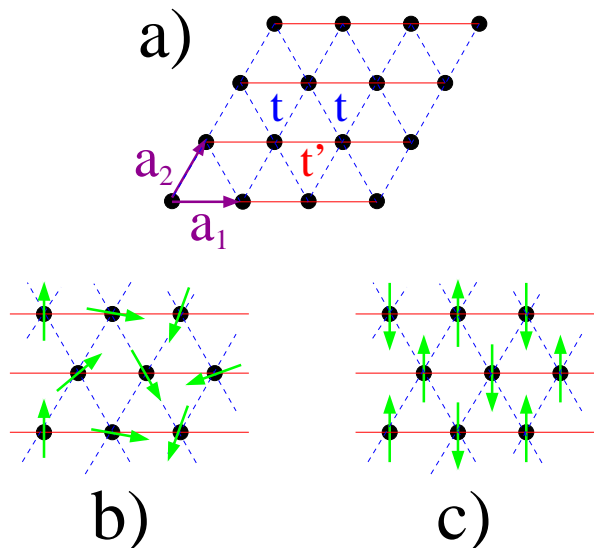


FIG. 1: (Color on-line) Illustration of the anisotropic triangular lattice (a); solid and dashed lines denote hopping amplitudes t' and t , respectively. Spin patterns for the spiral with $\theta' = 2\theta$ (b) and for collinear (c) states.

In the following, we consider clusters with periodic boundary conditions defined by the vectors $\mathbf{T}_1 = l\mathbf{a}_1$ and $\mathbf{T}_2 = l\mathbf{a}_2$, in order to have $l \times l$ lattices with $L = l^2$ sites. The half-filled case, which is relevant for the aforementioned materials, is considered here.

One important difference between organic salts and $\text{Cs}_2\text{CuCl}_{4-x}\text{Br}_x$ is the degree of frustration given by the ratio between inter- and intra-chain couplings. In the case of organic salts, $t'/t < 1$, thus implying a truly two-dimensional (frustrated) lattice geometry; by contrast, in the case of $\text{Cs}_2\text{CuCl}_{4-x}\text{Br}_x$, $t'/t < 1$, thus leading to a more one-dimensional (but frustrated) regime. When considering the strong-coupling limit, the comparison between neutron scattering experiments and theoretical calculations suggested that the ratio between inter- and intra-chain super-exchange couplings is $J/J' \simeq 0.74$ and 0.33 for Cs_2CuBr_4 ¹¹ and Cs_2CuCl_4 ,⁸ respectively, while the interlayer coupling J_\perp in Cs_2CuCl_4 is estimated to be smaller than $10^{-2}J$. Similar values for J and J' in both materials have been also found from the temperature dependence of the magnetic susceptibility.¹² Going back to the Hubbard model, these ratios are equivalent to $t/t' \simeq 0.86$ and 0.57 , mostly in agreement with a density-functional theory (DFT) study of microscopic models for these compounds.⁹ By using electron spin resonance spectroscopy, very recent evaluations of the super-exchange couplings suggested smaller values of J/J' in both Br and Cl compounds, i.e., $J/J' \simeq 0.4$ and 0.3 , respectively.¹³ Despite quantitative differences in the super-exchange couplings (especially for the Br compound), all these observations indicate that Cs_2CuCl_4 is more one-dimensional than Cs_2CuBr_4 .

Here, we focus our attention on the region with $t/t' <$

1, completing our recent work that analyzed the opposite case with $t'/t < 1$.^{14–16} As discussed above, the region $t/t' < 1$ is suitable for describing $\text{Cs}_2\text{CuCl}_{4-x}\text{Br}_x$. Although these systems are Mott insulators with electrons almost fully localized on Copper atoms, investigating the insulating behavior and a possible metal-to-insulating transition with the more general Hubbard model may unveil unforeseen new phenomena driven by the interplay of strong correlation and frustration; these aspects, as described below, have been only marginally investigated in the past.

A substantial body of theoretical work has treated the anisotropic triangular lattice in the region $0 \leq t/t' \leq 1$, however mostly in the infinite- U limit, i.e., when only spin degrees of freedom are present. For quasi-one-dimensional lattices, it has been suggested that spins may display a collinear pattern, in sharp contrast with what is found in the classical limit,¹⁷ where spins of neighboring chains form an angle of 90 degrees. This claim has been originally proposed by a renormalization group approach,¹⁸ and then supported by density-matrix renormalization group (DMRG) calculations on a three-leg spin tube.¹⁹

Incommensurate magnetism has been suggested by a functional renormalization group study to appear in a small region close to the isotropic point, with a spin-liquid state characterized by commensurate magnetic correlations being stabilized when moving towards the one-dimensional limit.²⁰ The existence of an essentially one-dimensional spin liquid phase in a wide regime of inter-chain couplings has been also obtained by the variational Monte Carlo approach, based upon Gutzwiller projected mean-field states.^{21–23} A relatively extended one-dimensional disordered phase has been also suggested by exact diagonalizations²⁴ and by spin-wave approaches,²⁵ while a one-dimensional dimer phase comes out from the $\text{SU}(N)$ Hubbard-Heisenberg model, solved in the large- N limit.²⁶ DMRG calculations using pinned fields on the boundaries found incommensurate spin-spin correlations all the way from the isotropic point to the limit of decoupled chains,²⁷ suggesting a more classical scenario with a pitch vector that continuously changes with J/J' . In this respect, also Dzyaloshinskii-Moriya interactions have been proposed to be relevant in stabilizing spiral magnetic order with respect to the collinear one.²⁸

In contrast to the Heisenberg-model investigations, not so many studies have been performed directly on the Hubbard model on the anisotropic triangular lattice for $t/t' < 1$. We mention mean-field²⁹ and variational Monte Carlo³⁰ approaches, suggesting a magnetically ordered ground state for large on-site interactions. Instead, calculations within the variational cluster approximation suggested that an extended spin-liquid phase may be present close to the isotropic point $t = t'$.^{31–33} Finally, a possible spin-liquid region close to the metal-insulator transition has been suggested for the Hubbard model on the isotropic point, for example by the strong-coupling approach of Ref. [34].

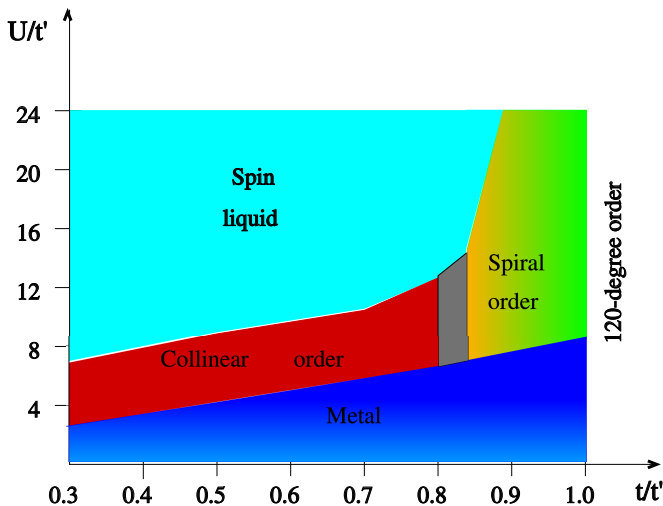


FIG. 2: (Color online) Schematic phase diagram of the Hubbard model on the anisotropic triangular lattice with $t/t' < 1$, as obtained by variational Monte Carlo. In the spiral-order region, the optimal pitch angle ranges from 0.6π to $2\pi/3$, with the 120° ordered state $\theta = 2\pi/3$ being stable at the isotropic point. In the gray region $0.8 \lesssim t'/t \lesssim 0.85$ the nature of the magnetic order cannot be reliably determined.

Here, we consider improved variational wave functions, pursuing the approach used previously¹⁵ to study the case with $t'/t < 1$. In order to consider the relevant phases that have been proposed for the Heisenberg model, we take into account correlated variational wave functions that may describe magnetic and spin-liquid states, as well as metallic or superconducting phases. In particular, concerning the magnetic case, we consider both wave functions having collinear magnetic correlations as well as states with spiral order, where the latter ones are constructed by starting from the states obtained at the Hartree-Fock level^{35,36} and including, in a second step, many-body correlations. In this way, we are able to treat different magnetic and non-magnetic states on the same level and determine which state is stabilized for a given value of frustration t/t' and Coulomb repulsion U . We would like to mention that variational approaches may contain, as a matter of principle, a bias towards ordered states. However, very accurate results are obtained in a wide regime of frustration when using, as in the present work, generalized Gutzwiller wave functions with long-range Jastrow terms and backflow corrections.^{37,38}

The paper is organized as follows: in section II, we discuss the form of the variational wave functions used in this work; in section III, we present our numerical calculations; finally, in section IV, we draw the conclusions.

II. NUMERICAL METHODS

The variational wave functions that are used to draw the phase diagram as a function of t/t' and U/t' are given

by:

$$|\Psi\rangle = \mathcal{J}_s \mathcal{J}_d |\Phi_0\rangle, \quad (2)$$

where \mathcal{J}_s and \mathcal{J}_d are conventional spin-spin and density-density Jastrow terms:

$$\mathcal{J}_s = \exp \left[\frac{1}{2} \sum_{i,j} u_{i,j} S_i^z S_j^z \right], \quad (3)$$

$$\mathcal{J}_d = \exp \left[\frac{1}{2} \sum_{i,j} v_{i,j} n_i n_j \right], \quad (4)$$

$u_{i,j}$ and the $v_{i,j}$ (that includes the on-site Gutzwiller term $v_{i,i}$) are pseudo-potentials that can be optimized for every independent distance $|\mathbf{R}_i - \mathbf{R}_j|$ in order to minimize the variational energy and S_i^z is the z -component of the spin operator on site i . $|\Phi_0\rangle$ is constructed starting from a generic mean-field Hamiltonian and then considering backflow correlations.^{37,38} In particular, we will consider two possible mean-field Hamiltonians in order to describe either magnetic or paramagnetic states.

As far as the former ones are concerned, we perform the unrestricted Hartree-Fock decoupling of Eq. (1) as described in Ref. [15]. We then obtain the decoupled Hamiltonian:

$$\begin{aligned} \mathcal{H}_{\text{AF}} = & - \sum_{i,j,\sigma} t_{ij} c_{i,\sigma}^\dagger c_{j,\sigma} + \text{h.c.} \quad (5) \\ & + U \sum_i [(n_{i,\downarrow})n_{i,\uparrow} + \langle n_{i,\uparrow} \rangle n_{i,\downarrow}] \\ & - U \sum_i [\langle c_{i,\uparrow}^\dagger c_{i,\downarrow} \rangle c_{i,\downarrow}^\dagger c_{i,\uparrow} + \langle c_{i,\downarrow}^\dagger c_{i,\uparrow} \rangle c_{i,\uparrow}^\dagger c_{i,\downarrow}] \\ & - U \sum_i [\langle n_{i,\uparrow} \rangle \langle n_{i,\downarrow} \rangle - \langle c_{i,\uparrow}^\dagger c_{i,\downarrow} \rangle \langle c_{i,\downarrow}^\dagger c_{i,\uparrow} \rangle], \end{aligned}$$

This Hamiltonian contains $4L$ independent mean-field parameters: $\langle n_{i,\uparrow} \rangle$, $\langle n_{i,\downarrow} \rangle$, $\langle c_{i,\uparrow}^\dagger c_{i,\downarrow} \rangle$, and $\langle c_{i,\downarrow}^\dagger c_{i,\uparrow} \rangle$ for $i = 1, \dots, L$ which have to be computed self-consistently. We impose the spin order to be coplanar in the x - y plane, i.e., we look for solutions with $\langle n_{i,\uparrow} \rangle = \langle n_{i,\downarrow} \rangle$, which reduces the number of independent parameters to $3L$. The ground state is then obtained by diagonalizing the mean-field Hamiltonian (5).

In general, a regular spin pattern in the x - y plane can be described by two angles θ and θ' , defining the relative orientation of two neighboring spins along \mathbf{a}_2 and \mathbf{a}_1 , respectively. Here, we focus on the insulating region of the phase diagram where, according to previous calculations for the Heisenberg model,¹⁷ the optimal Hartree-Fock solutions display a spiral magnetic order, which may be parametrized through a single angle $\theta \in [\pi/2, 2\pi/3]$, with $\theta' = 2\theta$, see Fig. 1(b). A pitch angle of $\theta = 2\pi/3$ corresponds to the 120° order, suitable for $t = t'$, while $\theta = \pi/2$ corresponds to antiferromagnetic order along the chains with hopping t' , the spins of neighboring chains forming an angle of 90° (appropriate for the limit $t \rightarrow 0$). Besides this class of spiral states, we

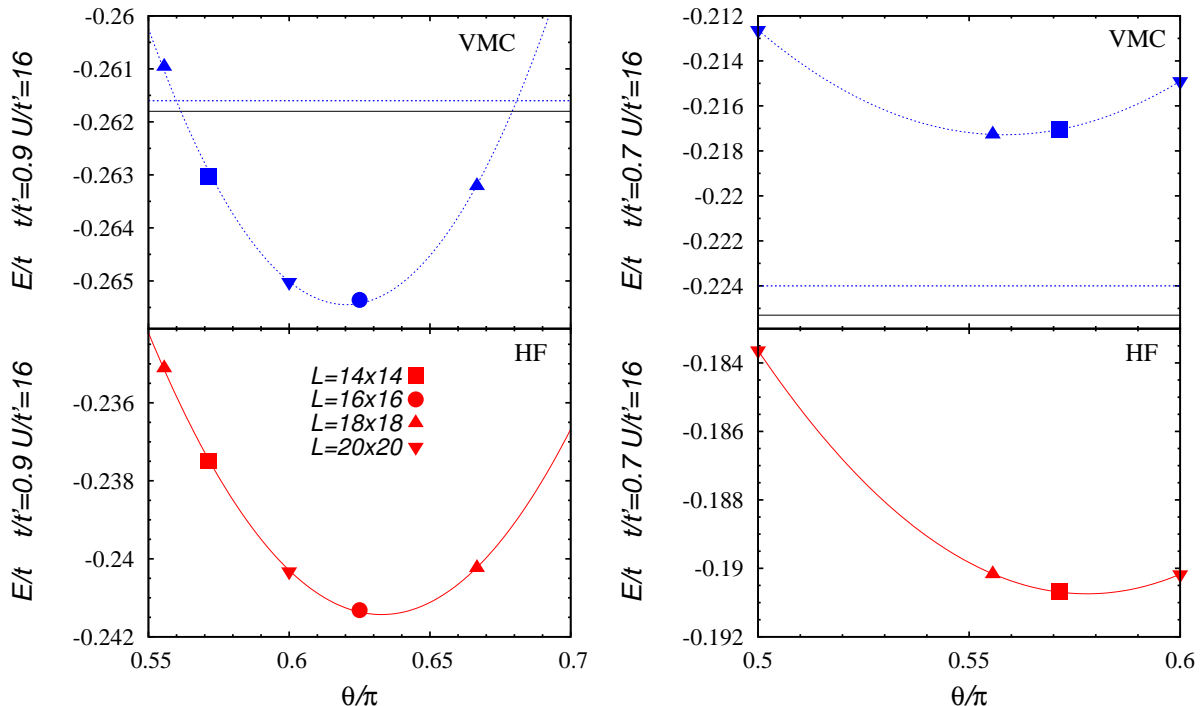


FIG. 3: (Color on-line) Upper panels: Variational Monte Carlo energies of the spiral state as a function of the pitch angle θ for $U/t' = 16$ and $t/t' = 0.9$ (left panels) and $t/t' = 0.7$ (right panels). We show data for the largest lattice size to which each angle may be accommodated. Lower panels: the same as in the upper panels, but for the Hartree-Fock calculations. In the upper panels, we also show for comparison the energy of the spin-liquid (horizontal solid black line) and of the collinear state (horizontal dotted blue line) on an $L = 18 \times 18$ lattice size.

also consider states with collinear order, i.e., with $\theta' = \pi$ and $\theta = 0$ or π , see Fig. 1(c).

We would like to mention that, in principle, also states with generic angles θ and θ' would be possible; however, as shown in Sec. III, we do not find any insulating region of the phase diagram where they give lower energies than the previous two magnetic states with $\theta' = 2\theta$ or with collinear patterns. Moreover, we do not find any evidence of a metallic phase with magnetic order.

Within this class of wave functions, both the spin and density Jastrow factors of Eqs. (3) and (4) are important for the correct description of the low-energy properties. In particular, the spin term is fundamental to reproduce the spin-wave fluctuations above the mean-field state.^{39,40}

For the non-magnetic states (both metallic and insulating), we consider an uncorrelated wave function given by the ground state of a BCS Hamiltonian:^{41–44}

$$\mathcal{H}_{\text{BCS}} = \sum_{k,\sigma} \xi_k c_{k,\sigma}^\dagger c_{k,\sigma} + \sum_k \Delta_k c_{k,\uparrow}^\dagger c_{-k,\downarrow}^\dagger + \text{h.c.}, \quad (6)$$

where the free-band dispersion ξ_k and the pairing ampli-

tude Δ_k are parametrized in the following way:

$$\xi_k = -2\tilde{t}' \cos(\mathbf{k} \cdot \mathbf{a}_1) - 2\tilde{t} [\cos(\mathbf{k} \cdot \mathbf{a}_2) + \cos(\mathbf{k} \cdot \mathbf{a}_3)] - \mu, \quad (7)$$

$$\Delta_k = 2\Delta' \cos(\mathbf{k} \cdot \mathbf{a}_1) + 2\Delta [\cos(\mathbf{k} \cdot \mathbf{a}_2) + \cos(\mathbf{k} \cdot \mathbf{a}_3)], \quad (8)$$

with the effective hopping amplitude \tilde{t} , the effective chemical potential μ , and the pairing fields Δ and Δ' being variational parameters to be optimized (\tilde{t}' gives the scale of energy of the mean-field Hamiltonian). In spite of the fact that we checked various symmetries for the pairing term, including both complex and non-translational invariant possibilities (see below), the best pairing function of Eq. (8) is found to have the $s + d_{xy}$ symmetry²⁹ in all the range $t/t' < 1$. In this regard, the symmetry of the variational state that is optimized in presence of backflow and Jastrow terms agrees with previous calculations treating simpler wave functions.^{29,30}

In this case, we do not consider the spin Jastrow factor (3), since we do not want to break the spin $\text{SU}(2)$ symmetry, retaining only density correlations (4). The latter ones allow to obtain a non-magnetic Mott insulator for a sufficiently singular Jastrow factor $v_q \propto 1/q^2$ (v_q being the Fourier transform of $v_{i,j}$), while $v_q \propto 1/q$ is found in a metallic/superconducting phase.^{45,46} The wave function for the spin-liquid phase is the generaliza-

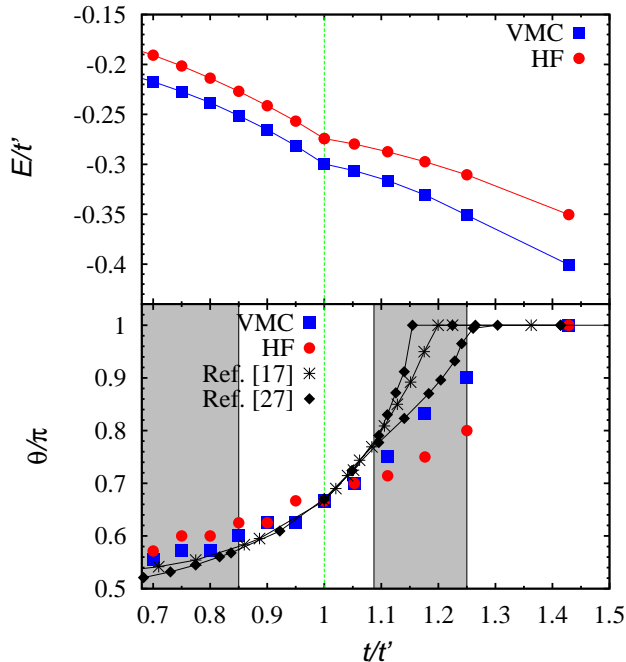


FIG. 4: (Color online) Upper panel: Hartree-Fock (red circles) and variational (blue squares) energies of the optimal spiral state as a function of t/t' for $U/t' = 16$. Lower panel: the pitch angle θ (in unit of π) of the optimal spiral state as a function of t/t' for $U/t' = 16$. The data for $t > t'$ are taken from Ref. [15]. The vertical line denotes the isotropic point with $t = t'$ and $\theta = 2\pi/3$. The gray regions denote the values of t/t' where, according to variational Monte Carlo calculations at $U/t' = 16$, the spin-liquid state has an energy lower than the spiral one. Together with our Hartree-Fock and variational Monte Carlo calculations, we show for comparison the results for the Heisenberg model from Ref. [17] and from Ref. [27]. In the latter case, two different sets of data are shown in the regime $t/t' > 1$, corresponding to $4n$ and $4n+2$ widths of the cylinders that are used in the DMRG calculations.

tion to the Hubbard model of the fully-projected BCS state that has been introduced by Anderson to describe the so-called resonating valence bond (RVB) state in the Heisenberg model.⁴⁷

We finally point out that the mean-field states obtained from Eqs. (5) and (6) are supplemented by back-flow terms, where each orbital that defines the unprojected states is taken to depend upon the many-body configuration, in order to incorporate virtual hopping processes.^{37,38} This procedure is a size-consistent and efficient way to improve the correlated wave functions on the lattice. Given the presence of Jastrow and back-flow terms, the optimization of the variational wave functions by energy minimization and the calculations of all physical quantities must be performed by using quantum Monte Carlo techniques.⁴⁸

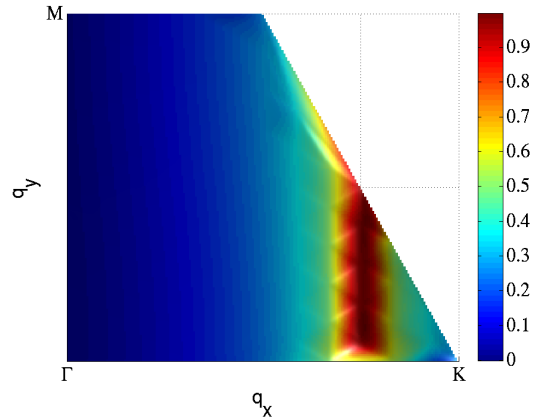


FIG. 5: (Color online) Spin structure factor $S(q)$ computed with the spin-liquid wave function for $t/t' = 0.6$ and $U/t' = 16$. Results are reported in the first quarter of the Brillouin zone, $\Gamma = (0, 0)$, $\mathbf{K} = (4\pi/3, 0)$, and $\mathbf{M} = (0, 2\pi/\sqrt{3})$.

III. RESULTS

The ground-state phase diagram as a function of the inter-chain hopping t and of the Coulomb interaction U is reported in Fig. 2, as obtained by comparing the energies of magnetic and non-magnetic wave functions. For small electron-electron interaction U/t' the ground state is metallic, the best state is obtained by starting from the mean-field *ansatz* of Eq. (6) with very small pairing terms Δ and Δ' and $v_q \propto 1/q$.

The ground state turns out to be insulating for larger values of U/t' , being either a spin liquid or magnetic. In the former case, the wave function is still described by the BCS *ansatz*, with sizable pairing having an $s + d_{xy}$ symmetry and $v_q \propto 1/q^2$. In the latter case, the best variational state is constructed starting from the magnetic mean field (5) that may have spiral or collinear order, with the collinear one being stabilized in a wide region for $t/t' \lesssim 0.8$. In the following, we describe in detail the properties of the different phases.

We point out that, on finite-size lattices with periodic-boundary conditions, only the set of pitch angles commensurate with the lattice size is accessible. Nonetheless, it is possible to reach a quite detailed understanding in the evolution of the wave vector describing ordered states. For $l \times l$ clusters, the allowed values are $\theta = 2\pi n/l$, with n being an integer. In this work, we will use lattice sizes ranging from 14×14 to 20×20 .

A. Magnetic states

We find that in a remarkably wide region, i.e., for $t/t' \lesssim 0.8$, the collinear state has a variational energy that is lower than the spiral wave function, while for $0.8 \lesssim t/t' \leq 1$ the spiral state is lower in energy. The optimal pitch angle is obtained by looking for the low-

est energy state among a set of angles close to the value predicted by Hartree-Fock, see Fig. 3. We have also verified that states with non-trivial generic angles θ and θ' do not provide a lower variational energy in the intermediate regime $t/t' \simeq 0.8$,

Collinear and spiral states are not connected continuously and a first-order phase transition could consequently occur between them; however, we cannot exclude that a very sharp crossover (with generic angles θ and θ') appear in a narrow region around $t/t' \simeq 0.8$. The energies are too close to allow a reliable discrimination.

In Fig. 4, we present the evolution of the energy and of the pitch angle θ of the optimal spiral state as a function of t/t' for $U/t' = 16$, in the range where spiral order is relevant. The energy gain when Jastrow and backflow corrections are added to the mean-field wave function is non-negligible (about $0.03t'$ independently from t). Most importantly, the pitch angle is only slightly affected by the inclusion of electron correlations through the Jastrow and the backflow terms for $t/t' < 1$. This behavior is quite different from the case with $t'/t < 1$, which we also include in Fig. 4, where the correlation factors renormalize the mean-field angle more strongly.¹⁵

B. Spin-liquid state

After optimization, the paramagnetic *ansatz* has vanishingly small pairing terms for small Coulomb interactions, leading to a metallic phase for $U < U_c(t)$; as expected, we find that $U_c(t) \rightarrow 0$ for $t/t' \rightarrow 0$, monotonically increasing up to the isotropic point $t = t'$, where $U_c(t = t') \simeq 8.5$.⁴⁹ By increasing the electron interaction, the paramagnetic state turns insulating, because of the Jastrow factor that changes from $v_q \propto 1/q$ to $v_q \propto 1/q^2$. In this regime, the pairing terms Δ and Δ' of Eq. (8) become finite, with the $s + d_{xy}$ symmetry in all the range $t/t' < 1$; indeed, both complex or $d_{x^2-y^2}$ symmetries are never found to be optimal. These results are in good agreement with previous variational Monte Carlo calculations,³⁰ where however a small region with $d_{x^2-y^2}$ symmetry has been obtained close to the isotropic point. This discrepancy could be due to the more accurate treatment of electronic correlations in our approach.

Our result contrasts with variational calculations on the Heisenberg model, where two different spin liquids have been proposed, one with $s + d_{xy}$ symmetry for small frustrating regimes and another with a 2×1 unit cell close to the isotropic point.²¹ Instead, in the Hubbard model, the *ansatz* with an extended 2×1 unit cell in the mean-field state cannot be stabilized for finite electron-electron repulsion. We emphasize that, within the Heisenberg model, the energy difference between these two wave functions is very small (about $0.001J'$) and, therefore, it is highly probable that in the presence of density fluctuations the more symmetric state that does not break translational symmetry is preferred.

We would like to point out that the spin-liquid state

has strong one-dimensional features. Indeed, typical ratios for the pairings Δ and Δ' are never larger than 0.1 for a wide range of inter-chain hoppings (i.e., for $0.1 \lesssim t/t' \lesssim 0.9$), indicating that the pairing occurs essentially along the chains with hopping t' . The relative sign of Δ and Δ' changes around $t/t' = 0.5$, with $\Delta/\Delta' > 0$ for $t/t' < 0.5$ and $\Delta/\Delta' < 0$ for $t/t' \geq 0.5$; nevertheless, the mean-field spectrum is always gapless at four Dirac points, with the precise location of the Dirac points being dependent on the optimal value of the variational parameters. The one-dimensional nature of the spin-liquid phase is further confirmed by looking at the spin-spin correlations for the variational state:

$$S(q) = \frac{1}{L} \sum_{m,l} e^{iq(m-l)} \langle S_m^z S_l^z \rangle, \quad (9)$$

where S_m^z is the z -component of the spin operator on site m . Results are reported for $t/t' = 0.6$ and $U/t' = 16$, which is well inside the spin-liquid region, in Fig. 5. $S(q)$ exhibits an extended line of maxima with $q_x = \pi$, clearly indicating the one-dimensional character of the wave function. This fact is particularly remarkable given the relatively large inter-chain hopping. Moreover, these maxima do not diverge with L , showing that only short-range order is present. A strong one-dimensional character of the spin-liquid phase comes out also from a mean-field study based upon Majorana fermions.⁵⁰ A very anisotropic magnon dispersion has been also proposed by a series expansion calculation.⁵¹

It is important to stress the fact that the existence of the spin-liquid phase is due to the presence of a frustrating hopping t between the chains. Indeed, if one-dimensional chains were coupled with an unfrustrated hopping, such to form an anisotropic square lattice with $t_x \neq t_y$, all the insulating phase would be immediately ordered with a commensurate Néel order.

C. Renormalization of the Fermi surface

We present now some results on the properties of the Fermi surface in the metallic phase, as well as the underlying Fermi surface in the insulating part of the phase diagram. In the upper panels of Fig. 6, we report the Fermi surface $\xi_k = 0$ in the metallic phase, close to the metal-insulator transition, for three values of the ratio t/t' , compared to the non-interacting case at $U = 0$. Our results show only a weak renormalization of the Fermi surface, due to interaction.

However, we would like to remark that the spin-spin correlations $S(q)$, defined in Eq. (9), show a tendency toward one-dimensionality when increasing the Coulomb repulsion U also in the metallic phase, see Fig. 7. This result suggests that, even though the renormalization of the Fermi surface is quite small in the metallic phase, this is sufficient to induce a noticeable change of the spin-spin structure factor.

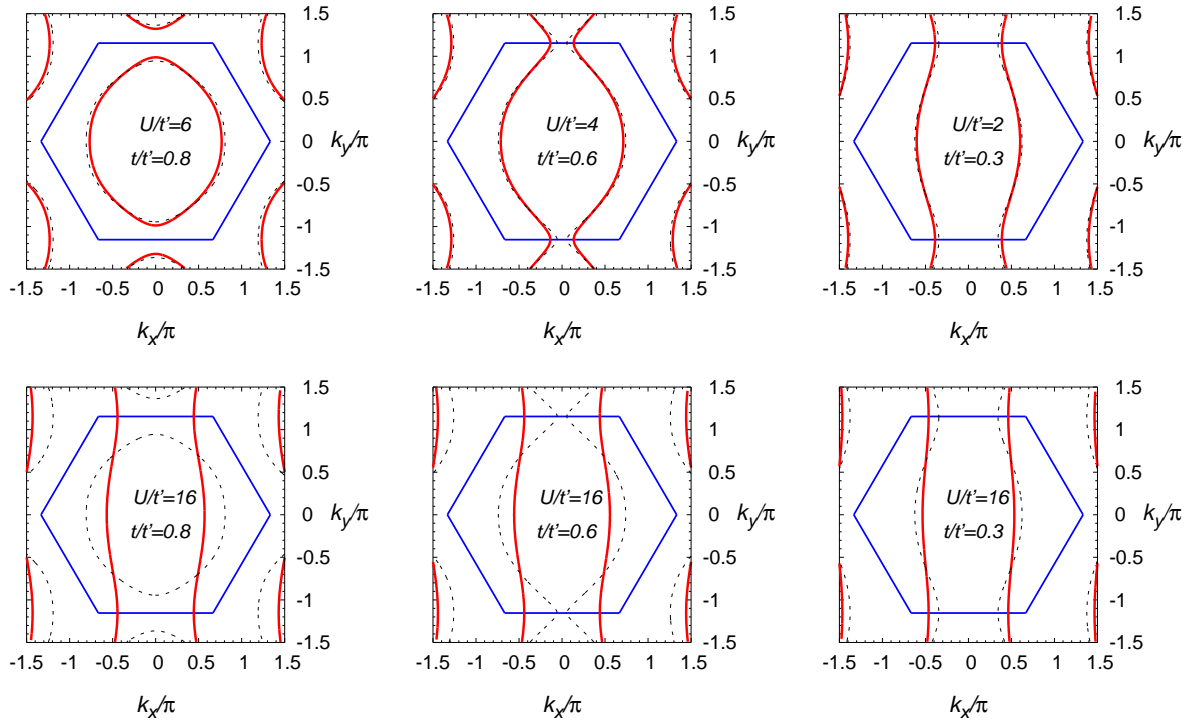


FIG. 6: (Color online) Upper panels: Fermi surface in the metallic phase (solid red lines) compared to the non-interacting results at $U = 0$ (dashed black lines). Data are shown for three different values of t/t' , close to the metal-insulator transition. Lower panels: Underlying Fermi surface in the spin-liquid region (solid red lines) compared to the non-interacting results (dashed black lines). Data are shown at $U/t' = 16$, for three different values of t/t' . The Brillouin zone of the triangular lattice is marked by blue lines.

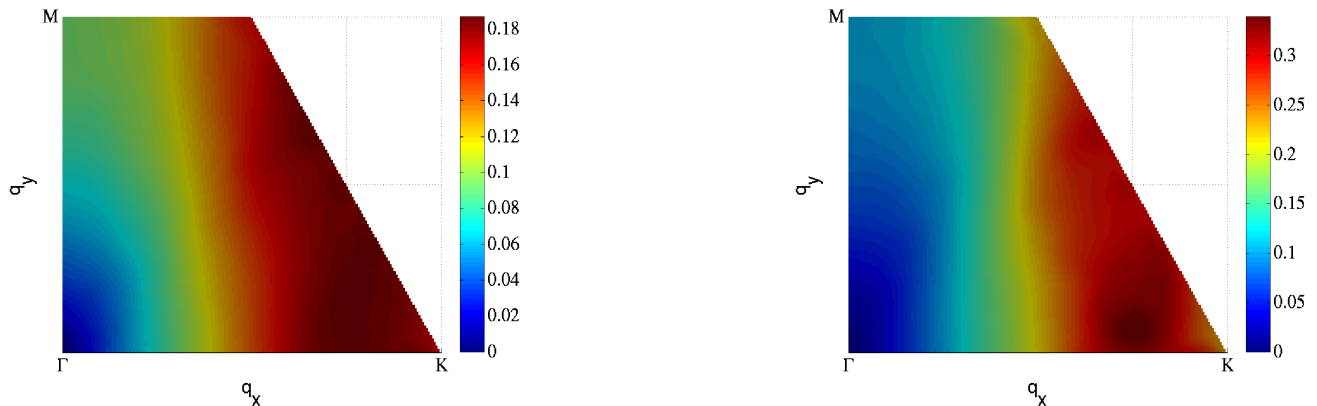


FIG. 7: (Color online) Spin-spin correlations $S(q)$ in the metallic phase for $U = 0$ and $t/t' = 0.6$ (left panel) and for $U/t' = 4$ and $t/t' = 0.6$ (right panel). Results are reported in the first quarter of the Brillouin zone, $\Gamma = (0, 0)$, $\mathbf{K} = (4\pi/3, 0)$, and $\mathbf{M} = (0, 2\pi/\sqrt{3})$.

The concept of Fermi surface can be also generalized to systems that become gapped because of some symmetry breaking or electronic correlation, leading to the idea of an underlying Fermi surface.⁵² Within our variational approach, the underlying Fermi surface can be easily defined and corresponds, like in the metallic phase, to the locus of the highest occupied momenta $\xi_k = 0$,

when the pairing is set to zero.⁵³ The lower panels of Fig. 6 show that the underlying Fermi surface in the spin-liquid region is strongly renormalized compared to the non-interacting case, leading to a quasi one-dimensional behavior. This result suggests that the collinear phase appearing at intermediate values of U/t' may be due to an instability of the spin-liquid region, and thus being a

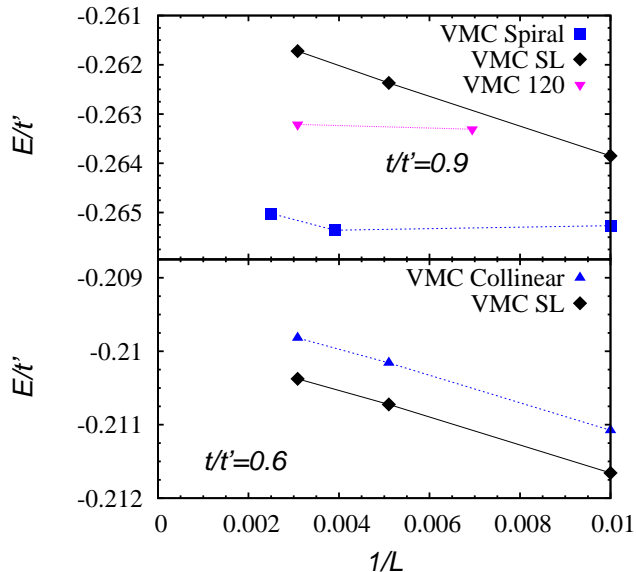


FIG. 8: (Color online) Upper panel: variational energies of the optimal spiral (blue squares) and spin-liquid (black diamonds) states as a function of the inverse system size $1/L$, for $U/t' = 16$ and $t/t' = 0.9$. The energy of the 120° order with $\theta = 2\pi/3$ is shown for comparison. Lower panel: variational energies of the collinear (blue triangles) and spin-liquid (black diamonds) states as a function of the inverse system size $1/L$, for $U/t' = 16$ and $t/t' = 0.6$.

strong-coupling phenomenon.

D. Phase diagram

By comparing the energies of magnetic and non-magnetic wave functions, we can obtain the zero-temperature phase diagram reported in Fig. 2. Few remarks are necessary to clarify some aspects of it. First of all, as mentioned above, given the fact that only a limited number of pitch angles are available on finite clusters, relatively large size effects are seen for spiral states. In various cases, the energy per site is not monotonic with L , showing that the true angle may be captured by some clusters but not by others. Even if these oscillations are never huge, i.e., of the order of $0.001t'$ for the sizes considered here, this fact makes it difficult to determine the precise boundary between spirals and other phases.

Still, within our approach it is possible to obtain solid results in specific regimes. In particular, it is clear that a magnetically disordered phase is present for relatively large electron-electron interactions and intermediate inter-chain hoppings. As an example, for $t/t' = 0.6$ and $U/t' = 16$, the lowest variational energy is achieved by the spin liquid state with the BCS *ansatz*, see Fig. 8. Here, the energies for the spin-liquid state are compared with the ones of the collinear state as a function of the cluster size, the spiral state being much higher in en-

ergy for all possible pitch angles (see Fig. 3). This is the typical outcome that appears for $U/t' \gtrsim 10$ and $0.3 \lesssim t/t' \lesssim 0.8$.

When the ratio t/t' is reduced, the situation becomes less clear, since close to the one-dimensional limit both the collinear and the BCS states are very close in energy. For example, for $t/t' = 0.1$ we obtain $E/t' = -0.3269(1)$ (for $U/t' = 8$) and $E/t' = -0.1715(1)$ (for $U/t' = 16$) for both variational *ansätze*; therefore, we cannot determine whether the spin-liquid phase persists down to $t \rightarrow 0$ or not. We should point out that since for $t/t' = 0.1$ the spin-liquid phase is not any more energetically favored at large values of U/t' , our results do not exclude that the ground state of the Heisenberg model close to the one-dimensional limit has (collinear) magnetic order, as predicted by Refs. [18,19]. It must be also emphasized that, in the one-dimensional limit both the BCS and the collinear state do not possess magnetic long-range order, since here the fluctuations generated by the Jastrow factor are sufficient to destroy the order present at the mean-field level.³⁹ On the other hand, whenever a coupling between chains is present, the magnetic order should not be destroyed by the Jastrow factor.

For $t/t' \gtrsim 0.9$, the wave function with spiral order becomes competitive with both spin-liquid and collinear ones for a non trivial angle θ/π that is about 0.6. The trend is clear despite pronounced size effects, that are due to the relatively small number of angles that are commensurate with the lattice size, see Figs. 3 and 8.

IV. CONCLUSIONS

In summary, we analyzed the half-filled Hubbard model on the anisotropic lattice in the range of parameters $t/t' < 1$ by considering variational wave functions that include both Jastrow and backflow terms and are able to describe spin-liquid and magnetic states with different pitch vectors on the same footing. For large values of the interaction U/t' and moderate to large inter-chain hoppings $0.3 \lesssim t/t' \lesssim 0.8$ a spin-liquid state with strong one-dimensional features and four Dirac points stabilizes with respect to any magnetic state considered here. However, close to the isotropic point, magnetic states with non trivial spiral order are more favorable. Interestingly, close to the metal-insulator transition, a collinear order stabilizes in a wide region of t/t' , in sharp contrast with what is found in the classical limit. Our calculations are also relevant for the experimental results on the compounds Cs_2CuBr_4 and Cs_2CuCl_4 , showing that in the strong coupling regime spiral magnetic order is stabilized close to the isotropic point, while a spin-liquid state emerges for smaller values of t/t' .

Acknowledgments

We thank H. Feldner for providing the Hartree-Fock code and A. Weichselbaum for the DMRG data shown in Fig. 4. L.F.T., C.G. and R.V. acknowledge support by the German Science Foundation through the grant

SFB/TRR49. F.B. and L.F.T. thank partial support from PRIN 2010-11. R.V. and F.B. acknowledge the KITP program *Frustrated Magnetism and Quantum Spin Liquids: From Theory and Models to Experiments* and the National Science Foundation under Grant No. NSF PHY11-25915.

-
- ¹ P. Fazekas and P.W. Anderson, *Phil. Mag.* **30**, 423 (1974).
² ET=BEDT-TTF stands for bis(ethylenedithio)-tetrathiafulvalene. dmit is 1,3-dithiole-2-thione-4,5-dithiolate.
³ K. Kanoda and R. Kato, *Annual Rev. of Condens. Matter Phys.* **2**, 167 (2011).
⁴ B.J. Powell and R.H. McKenzie, *Rep. Prog. Phys.* **74**, 056501 (2011).
⁵ H.C. Kandpal, I. Opahle, Y.-Z. Zhang, H.O. Jeschke, R. Valenti, *Phys. Rev. Lett.* **103**, 067004 (2009).
⁶ K. Nakamura, Y. Yoshimoto, T. Kosugi, R. Arita, and M. Imada, *J. Phys. Soc. Jpn.* **78**, 083710 (2009).
⁷ T. Ono, H. Tanaka, O. Kolomiyets, H. Mitamura, T. Goto, K. Nakajima, A. Oosawa, Y. Koike, K. Kakurai, J. Klenke, P. Smeibidle and M. Meissner, *J. Phys.: Condens. Matter* **16**, S773 (2004).
⁸ R. Coldea, D.A. Tennant, A.M. Tsvelik, and Z. Tylczynski, *Phys. Rev. Lett.* **86**, 1335 (2001); R. Coldea, D.A. Tennant, and Z. Tylczynski, *Phys. Rev. B* **68**, 134424 (2003).
⁹ K. Foyevtsova, I. Opahle, Y.-Z. Zhang, H.O. Jeschke, R. Valenti, *Phys. Rev. B* **83**, 125126 (2011).
¹⁰ P. T. Cong, B. Wolf, M. de Souza, N. Krueger, A.A. Haghighirad, S. Gottlieb-Schoenmeyer, F. Ritter, W. Assmus, I. Opahle, K. Foyevtsova, H.O. Jeschke, R. Valenti, L. Wiehl, and M. Lang, *Phys. Rev. B* **83**, 064425 (2011).
¹¹ T. Ono, H. Tanaka, T. Nakagomi, O. Kolomiyets, H. Mitamura, F. Ishikawa, T. Goto, K. Nakajima, A. Oosawa, Y. Koike, K. Kakurai, J. Klenke, P. Smeibidle, M. Meissner, and H. Aruga Katori, *J. Phys. Soc. Jpn.* **74**, 135 (2005).
¹² W. Zheng, R.R.P. Singh, R.H. McKenzie, and R. Coldea, *Phys. Rev. B* **71**, 134422 (2005).
¹³ S.A. Zvyagin, D. Kamenskyi, M. Ozerov, J. Wosnitza, M. Ikeda, T. Fujita, M. Hagiwara, A.I. Smirnov, T.A. Soldatov, A.Ya. Shapiro, J. Krzystek, R. Hu, H. Ryu, C. Petrovic, and M.E. Zhitomirsky, *Phys. Rev. Lett.* **112**, 077206 (2014).
¹⁴ L.F. Tocchio, A. Parola, C. Gros, and F. Becca, *Phys. Rev. B* **80**, 064419 (2009).
¹⁵ L.F. Tocchio, H. Feldner, F. Becca, R. Valenti, and C. Gros, *Phys. Rev. B* **87**, 035143 (2013).
¹⁶ A.C. Jacko, Luca F. Tocchio, H. O. Jeschke and R. Valenti, *Phys. Rev. B* **88**, 155139 (2013).
¹⁷ Z. Weihong, R.H. McKenzie, and R.R.P. Singh, *Phys. Rev. B* **59**, 14367 (1999).
¹⁸ O.A. Starykh and L. Balents, *Phys. Rev. Lett.* **98**, 077205 (2007).
¹⁹ R. Chen, H. Ju, H.-C. Jiang, O.A. Starykh, and L. Balents, *Phys. Rev. B* **87**, 165123 (2013).
²⁰ J. Reuther and R. Thomale, *Phys. Rev. B* **83**, 024402 (2011).
²¹ S. Yunoki and S. Sorella, *Phys. Rev. B* **74**, 014408 (2006).
²² Y. Hayashi and M. Ogata, *J. Phys. Soc. Jpn.* **76**, 053705 (2007).
²³ D. Heidarian, S. Sorella, and F. Becca, *Phys. Rev. B* **80**, 012404 (2009).
²⁴ M.Q. Weng, D.N. Sheng, Z.Y. Weng, and Robert J. Bursill, *Phys. Rev. B* **74**, 012407 (2006).
²⁵ P. Hauke, T. Roscilde, V. Murg, J.I. Cirac, and R. Schmied, *New J. Phys.* **13**, 075017 (2011).
²⁶ C.H. Chung, J.B. Marston, and R.H McKenzie, *J. Phys.: Condens. Matter* **13**, 5159 (2001).
²⁷ A. Weichselbaum and S.R. White, *Phys. Rev. B* **84**, 245130 (2011).
²⁸ S. Ghamari, C. Kallin, S.-S. Lee, and E.S. Sørensen, *Phys. Rev. B* **84**, 174415 (2011).
²⁹ B.J. Powell and R.H. McKenzie, *Phys. Rev. Lett.* **98**, 027005 (2007).
³⁰ T. Watanabe, H. Yokoyama, Y. Tanaka, and J. Inoue, *Phys. Rev. B* **77**, 214505 (2008).
³¹ P. Sahebsara and D. Senechal, *Phys. Rev. Lett.* **100**, 136402 (2008).
³² A. Yamada, *Phys. Rev. B* **89**, 195108 (2014).
³³ M. Laubach, R. Thomale, W. Hanke, and G. Li, arXiv:1401.8198
³⁴ H.-Y. Yang, A.M. Lauchli, F. Mila, and K.P. Schmidt, *Phys. Rev. Lett.* **105**, 267204 (2010).
³⁵ H.R. Krishnamurthy, C. Jayaprakash, S. Sarker, and W. Wenzel, *Phys. Rev. Lett.* **64**, 950 (1990).
³⁶ C. Pinettes and C. Lacroix, *Solid State Commun.* **85**, 565 (1993).
³⁷ L.F. Tocchio, F. Becca, A. Parola, and S. Sorella, *Phys. Rev. B* **78**, 041101 (2008).
³⁸ L.F. Tocchio, F. Becca, and C. Gros, *Phys. Rev. B* **83**, 195138 (2011).
³⁹ F. Franjic and S. Sorella, *Prog. Theor. Phys.* **97**, 399 (1997).
⁴⁰ F. Becca, M. Capone, and S. Sorella, *Phys. Rev. B* **62**, 12700 (2000).
⁴¹ C. Gros, *Phys. Rev. B* **38**, 931(R) (1988).
⁴² F.C. Zhang, C. Gros, T.M. Rice, and H. Shiba, *Supercond. Sci. Technol.* **1**, 36 (1988).
⁴³ C. Gros, *Annals of Physics* **189**, 53 (1989).
⁴⁴ B. Edegger, V.N. Muthukumar, and C. Gros, *Adv. Phys.* **56**, 927 (2007).
⁴⁵ M. Capello, F. Becca, M. Fabrizio, S. Sorella, and E. Tosatti, *Phys. Rev. Lett.* **94**, 026406 (2005).
⁴⁶ M. Capello, F. Becca, S. Yunoki, and S. Sorella, *Phys. Rev. B* **73**, 245116 (2006).
⁴⁷ P.W.A. Anderson, *Science* **235**, 1196 (1987).
⁴⁸ S. Sorella, *Phys. Rev. B* **71**, 241103 (2005).
⁴⁹ For a detailed comparison of different studies of the metal-insulator transition on the isotropic triangular lattice, see J. Kokalj and R.H. McKenzie, *Phys. Rev. Lett.* **110**, 206402 (2013).
⁵⁰ T. Herfurth, S. Streib, and P. Kopietz, *Phys. Rev. B* **88**, 174404 (2013).

⁵¹ J.O. Fjærestad, W. Zheng, R.R.P. Singh, R.H. McKenzie, and R. Coldea, Phys. Rev. B **75**, 174447 (2007).

⁵² I. Dzyaloshinskii, Phys. Rev. B **68**, 085113 (2003).

⁵³ L.F. Tocchio, F. Becca, and C. Gros, Phys. Rev. B **86**, 035102 (2012).